Identification of potential novel pharmaceutical targets against the development of right- and left-sided heart failure

Ph.D. Thesis

Author: Katalin Takács-Ördög

Program leader: Prof. Ferenc Gallyas Jr., D.Sc.

Project leader: Prof. Róbert Halmosi M.D., D.Sc.

1st Department of Medicine

University of Pécs, Medical School

Doctoral School of Interdisciplinary Medical Sciences

Hungary

2025

ABBREVIATIONS

ATP	adenosine triphosphate
BNP	B-type natriuretic peptide
DMEM	Dulbecco's modified Eagle Medium
Drp1	dynamine-related protein 1
ETC	electron transport chain
GAPDH	glyceraldehyde 3-phosphate dehydrogenase
HF	heart failure
IFM	interfibrillar mitochondria
L-2286	(2-[(2-Piperidine-11-yletil)thio]quinazolin-4(3H)-one)
LDH	lactate dehydrogenase
LV	left ventricle
MAPK	mitogen activated protein kinase
MCT	monocrotaline
Mfn 1/2	mitofusins 1 and 2
MQC	mitochondrial quality control
mtDNA	mitochondrial DNA
NRCM	neonatal rat cardiomyocytes
Opa1	optic atrophy 1
PAH	pulmonary arterial hypertension
PARP	poly(ADP-ribose) polymerase
PCR	polymerase chain reaction
PDH	pyruvate dehydrogenase
PH	pulmonary hypertension
PI3K	phosphoinositide 3-kinase
RAAS	renin-angiotensin-aldosterone system
RHF	right-sided heart failure
RIRR	ROS-induced ROS release
ROS	reactive oxygen species
SHR	sponatanously hypertensive rat
SNS	sympathetic nervous system
TGF-β	transforming growth factor β
WKY	Wistar Kyoto rat

1. INTRODUCTION

Heart failure (HF) is characterized by the inability of heart to provide adequate supply of blood and therefore oxygen and nutrients to various organs and peripheral tissues meeting their metabolic needs. Conventionally, the prevalence of heart failure in developed countries is thought to be approximately 2%, increasing to more than 10% in people over the age of 70. Heart failure still has a very poor prognosis despite the therapeutic advancements in the last several decades. Additionally, HF-related hospitalizations and mortality are increasing, placing a significant burden on healthcare systems and the economy. Therefore, the prevention of HF is of paramount importance. According to the ESC Guidelines, the etiology of heart failure can be divided into 3 main categories: diseased myocardium, abnormal loading conditions, and arrhythmias. Left-sided heart failure occurs when the left ventricle is unable to effectively pump blood to the systemic circulation. It can be further classified into 3 subgroups based on the left ventricular ejection fraction. LV systolic dysfunction is defined as an ejection fraction less than 40%, referred to as HF with a reduced ejection fraction (HFrEF). Patients with an ejection fraction between 41% and 49% have mildly reduced ejection LV systolic function (HFmrEF). The third subgroup includes patients with EF more than 50% (HF with preserved EF, HFpEF) when the left ventricle is stiff and cannot relax properly, resulting in impaired diastolic filling. Hypertension represents one of the primary and most common risk factors leading to the development of heart failure (HF) across the entire spectrum of the left ventricular ejection fraction. Right-sided heart failure occurs when the right ventricle is unable to pump blood efficiently into the pulmonary circulation. This leads to a congestion of blood in the veins, causing fluid accumulation, particularly in the lower extremities (edema), abdomen (ascites), and liver. The causes of right-sided heart failure can be divided broadly into 5 main categories: 1.) secondary to left ventricular failure (backward failure effect of LVH), 2.) secondary to primer or secondary pulmonary hypertension, 3.) RV and tricuspid valve pathologies, 4.) diseases of the pericardium, and 5.) congenital heart defects and systemic diseases. The most common cause of right-sided heart failure (RHF) is the backward effects of left ventricular failure including pulmonary hypertension (PH). The progression of RHF in pulmonary hypertension is driven mainly by the consequences of elevated RV afterload. While the pathophysiological mechanisms vary among different PH groups, a common factor is the effects of increased loading conditions on the RV.

1.1. Signaling pathways in cardiac remodeling

Ventricular remodeling refers to the structural and functional alterations in the heart that occur after a myocardial injury, potentially leading to HF. This process is driven by perturbations in various aspects, such as energy metabolism, excitation-contraction coupling, calcium handling, contractile proteins or their regulatory components, and cytoskeletal elements. In the failing heart, changes in the expression of genes associated with these functions may contribute to and accelerate the process of remodeling. Owing to their different functional requirements and structural characteristics, right and left ventricular remodeling differ not only in their physiological responses but also in the activation and utilization of signaling pathways. The neurohormonal systems, including the renin-angiotensin-aldosterone system (RAAS) and the sympathetic nervous system (SNS), play key roles in both left (LV) and right (RV) ventricles. Chronic activation of these pathways leads to maladaptive changes like fibrosis, hypertrophy, and apoptosis, exacerbating remodeling. Calcium handling disruptions, including impaired sarcoplasmic reticulum calcium reuptake, contribute to maladaptive hypertrophy. Key signaling pathways like MAPK, TGF-β/Smad, PI3K/Akt, and PARP also regulate fibrosis, cell survival, and inflammation, driving pathological changes. These alterations impair contractility and efficiency, eventually leading to HF.

1.2. Beyond conventional use: the cardiovascular protective potential of PARP inhibitors and colchicine

Poly(ADP-ribose) polymerase inhibitors have gained attention in oncologic diseases due to their pivotal role in DNA repair and cellular homeostasis. Originally developed for the treatment of cancers with defective homologous recombination repair (HRR), such as BRCA1/2-mutated breast and ovarian cancers. These inhibitors block the repair of single-strand DNA breaks, leading to synthetic lethality in tumor cells. These inhibitors have emerged as a significant therapeutic strategy in various cancers, particularly ovarian, breast, prostate, and pancreatic cancers. However, accumulating evidence suggests their potential extends beyond oncology, particularly in non-cancerous conditions related to inflammation, neuroprotection, and metabolic disorders. In the context of cardiovascular diseases, excessive PARP activation has been implicated in oxidative stress-induced cellular damage, particularly in conditions such as ischemia-reperfusion injury, heart failure and atherosclerosis. Our research group has previously demonstrated that pharmacological

PARP inhibition offers protection against the development of post-infarction, hypertension-induced, toxic heart failure, as well as hypertension-induced early cardiovascular damage (hypertensive heart disease), consistent with findings in other scientific studies.

Colchicine is a well-known anti-inflammatory drug with a long history of use in the treatment of gout and familial Mediterranean fever (FMF). Its mechanism of action primarily involves the disruption of microtubule polymerization, leading to the inhibition of neutrophil migration, cytokine release and inflammasome activation. In recent years, colchicine has shown promise in managing certain cardiovascular diseases, such as pericarditis, coronary artery disease, and heart failure. It has become a first-line adjunct therapy alongside NSAIDs or corticosteroids for preventing acute and recurrent pericarditis. Clinical trials (e.g., COLCOT, LoDoCo2) have also indicated its potential in treating coronary artery disease and atherosclerosis[83]. Its ability to suppress inflammation at multiple levels makes it a promising therapy for cardiovascular diseases, where inflammation plays a pivotal role.

Given the inflammatory and oxidative stress-driven nature of heart failure, both PARP inhibitors and colchicine represent promising therapeutic options for right- and left-sided heart failure. Investigating their effects could lead to novel targeted therapies that address the underlying molecular mechanisms of myocardial dysfunction, fibrosis, and energy deficiency.

1.3. Role of mitochondria in heart failure

Mitochondria are double-membrane-bounded organelles within cells and are often referred to as the "powerhouses" of eukaryotic cells. Mitochondria play a crucial role in continuously supplying energy while adapting to changing stimuli by converting various substrates into ATP. This metabolic flexibility allows the heart to respond to changes in oxygen levels, changes in the availability of nutrients in the bloodstream, and increased workload, e.g. during exercise. The oxidative phosphorylation (OXPHOS) system, located within the inner mitochondrial membrane, consists of five multiprotein complexes (I–V) and two mobile electron carriers: cytochrome c and coenzyme Q. Its primary function is to coordinate electron and proton transfer, leading to ATP synthesis. Mitochondria are highly adaptable organelles that can respond to cellular stressors and metabolic demands with remarkable plasticity and dynamism. This adaptability is the basis for their efficient regulation of a wide

variety of cellular functions. Mitochondrial quality control (MQC) is a set of interconnected processes that protect mitochondria from damage and prevent the accumulation of dysfunctional organelles. These processes include three main mechanisms: mitochondrial biogenesis, mitochondrial dynamics (fusion and fission), and mitophagy. Reactive oxygen species (ROS) production in mitochondria occurs primarily as a byproduct of oxidative phosphorylation during ATP synthesis. The central site of ROS generation is the electron transport chain (ETC) in the inner mitochondrial membrane. Complexes I and III are the main contributors to the formation of superoxide anions (O2•−), which are produced after a monoelectronic reduction of O_2 in mammalian cells. Reactive oxygen species (ROS) are highly reactive molecules with significant toxic potential, as they induce oxidative damage to critical cellular macromolecules. This includes peroxidation of lipids, oxidative modification of proteins, and mutagenic alterations to nucleic acids, leading to widespread cellular dysfunction. Oxidative stress occurs in cardiomyocytes when the production of ROS exceeds the capacity of the antioxidant defense system, leading to cellular damage. Under pathological conditions (e.g., hypoxia and I/R injury), a phenomenon known as ROS-induced ROS release (RIRR) has been observed. This feedback mechanism occurs when reactive oxygen species (ROS) production stimulates further ROS generation, thereby amplifying oxidative stress. Persistent ROS generation detrimentally affects mitochondrial function, leading to maladaptive cardiac remodeling, which is characterized by pathological hypertrophy and fibrosis and exacerbates disease progression.

1.4. Animal models in cardiovascular research

Spontaneously hypertensive rat (SHR) is a well-established animal model used extensively in cardiovascular research. These rats were originally developed in Japan in the 1960s by Professor Kyuzo Aoki and colleagues through the selective breeding of hypertensive Wistar rats. They mimic many aspects of human essential hypertension, including elevated blood pressure, increased risk of cardiovascular disease, and end-organ damage. Spontaneously hypertensive rats are born with normal blood pressure, typically in the range of 100–120 mmHg. Persistent hypertension, characterized by systolic blood pressure levels of 160–180 mmHg, develops at approximately 8–10 weeks of age and can rise to 240 mmHg in adults. After a prolonged period of stable hypertension and compensated cardiac hypertrophy, these animals begin to show signs of impaired cardiac function at approximately 40-50 weeks of age, predominantly affecting the left side of the heart. In SHRs, oxidative damage plays an

important role in the pathophysiology of hypertension and cardiovascular complications. In SHRs, increased production of reactive oxygen species (ROS), such as superoxide anions and hydrogen peroxide, overwhelms the body's antioxidant defenses. Therefore, the SHR strain is an excellent choice for studying hypertension-induced oxidative damage and left ventricular remodeling. Several preclinical animal models are available to study pulmonary arterial hypertension (PAH) and right ventricular failure. The most widely used model is the monocrotaline-induced pulmonary arterial hypertension rat model because of its simplicity, reproducibility, and cost-effectiveness. Monocrotaline (MCT), a pyrrolizidine alkaloid extracted from the plant *Crotalaria spectabilis*, is metabolized in the liver by the enzyme cytochrome P_{450}3A4 to produce an active pneumotoxic metabolite known as MCT pyrrole. This metabolite damages pulmonary artery endothelial cells, triggering complex pathological changes. This process effectively mimics several key aspects of human PAH, including vascular remodeling, inflammation, and right ventricular failure.

2. AIMS OF THE WORK

The aim of our first work was to examine the effects of PARP-inhibition using L-2286, on mitochondrial morphology and function in a chronic hypertension-induced heart failure model and an “in vitro” NRCM model.

a.) We aimed to investigate the effect of PARP-inhibition on LV hypertrophy and remodeling.

b.) We sought to examine the effects of L-2286 on IFM morphology and size distribution in an SHR model.

c.) Our goal was to study the effects of L-2286 on mitochondrial structure and function in an oxidative-stressed NRCM model.

d.) We aimed to clarify the effect of L-2286 on mitochondrial quality control processes in stressed cardiomyocytes.

In our second work, we aimed to clarify the effect of short-term low-dose colchicine treatment on pulmonary arterial hypertension in an MCT-induced PAH model.

e.) We sought to evaluate the effects of colchicine on pulmonary arterial remodeling and RV function.

f.) We aimed to study the role of colchicine treatment in the modulation of signaling pathways in the RV.

g.) We aimed to determine how colchicine affects the metabolic and inflammatory profile of the RV.

3. THE EFFECT OF PARP-INHIBITION ON MYOCARDIAL REMODELING

3.1. METHODS

3.1.1. IN VIVO MODEL

Ten-week-old male spontaneously hypertensive (SHR) and Wistar Kyoto (WKY) rats were purchased from Charles River Laboratories (Wilmington, MA, USA), and the animals were kept under standard conditions throughout the experiment; a 12 h light-dark cycle, water and rat chow were provided ad libitum. SHR rats were randomized into two groups: one group received no treatment (SHR-C, n=8), whereas the other group (SHR-L, n=8) received 5 mg/kg/day L-2286, a water-soluble PARP-inhibitor, for 32 weeks. The third was an age-matched normotensive control group (WKY, n=8). L-2286 was dissolved in the drinking water based on preliminary data about the volume of daily fluid consumption. Blood pressure measurements were performed on each animal on weeks 0 and 32 of the treatment period. All animals were examined by echocardiography to exclude rats with any heart abnormalities. Transthoracic two-dimensional echocardiography was performed under inhalation anesthesia at the beginning and the end of the study. At the end of the treatment period, all animals were sacrificed, and blood was collected to determine the concentration of plasma brain-derived natriuretic peptide (BNP), then hearts were removed. For electron microscopic analysis, hearts were perfused retrogradely through the aortic root with ice-cold PBS to wash away blood and then washed with a modified Kranovsky fixative. Total and fractionated Western blot samples were prepared from hearts to determine the expression level of mitochondrial dynamics-related proteins and their subcellular distributions.

3.1.2. IN VITRO MODEL

Cardiomyocytes were isolated from 1-3 days old neonatal Wistar rats via the Pierce™ Primary Cardiomyocyte Isolation Kit following the manufacturer's instructions. The animals were sacrificed, and their hearts were removed and minced into 1-3 mm^3 pieces. The pieces were digested with an enzyme complex (Cardiomyocyte Isolation Enzyme 1 (with papain) and Cardiomyocyte Isolation Enzyme 2 (with thermolysin)). Purified NRCMs were maintained in a humidified 5% CO_2 atmosphere at 37°C, and the cells were cultured in specific Dulbecco's modified Eagle's medium (DMEM) for primary cell isolation containing 10% fetal bovine serum (FBS) and antibiotic solution (1% penicillin and streptomycin solution). The following groups were created according to the applied treatment: Control group: cells without any treatment, L-2286 group: cells with only 10 μM

L-2286 for 0.5 hours, H_2O_2 group: cells with 150 μM H_2O_2 for 0.5 hours, H_2O_2+L-2286 group: cells with 150 μM H_2O_2 and 10 μM L-2286 for 0.5 hours. The expression levels of mitochondrial dynamics-related proteins and subcellular distribution were measured. The mitochondrial fragmentation and mitochondrial membrane potential were evaluated by fluorescent microscopes. The mitochondrial energy metabolism and function were measured with Agilent Seahorse assays. The mtDNA genome integrity was evaluated by real-time PCR and the citrate-synthase activity was measured using a kit from Sigma Aldrich following the manufacturer's instructions.

3.2. RESULTS

3.2.1. PARP-inhibition decreased left ventricular hypertrophy in spontaneously hypertensive rats

Table 1. Effects of L-2286 on echocardiographic parameters and BNP levels.

	WKY	SHR-C	SHR-L
EF (%)	70.24±1.12	67.21±1.22	69.13±1.84
LVEDV	280.78±9.93	350.78±11.02[a]	329.67±12.53[a,b]
LVESV	82.95±2.48	115.11±5.96[a]	101.32±3.34[a,b]
Septum	1.43±0.03	1.99±0.03[a]	1.72±0.04[a,b]
PW	1.45±0.02	2.05±0.02[a]	1.74±0.03[a,b]
LV weight (calc.)	978±17	1393±13[a]	1168±45[a,b]
SBP^{10w} (Hgmm)	130±5.4	182±5.6[a]	178±3.6[a]
SBP^{42w} (Hgmm)	128±4.8	231±6.3[a]	225±2.4[a]
HR (beats min^{-1})	308±13	339±7.8	335±9.2
VW/BW^{42w} (mg/g)	3.01±0.16	3.97±0.22[a]	3.38±0.3[a,b]
Lung wet weight/dry $weight^{42w}$	4.74±0.11	4.92±0.24	4.87±0.21
BNP (ng/mL)	2.06±0.15	2.35±0.03	2.23±0.13

WKY: 42-week-old normotensive age-matched animals, n=8; SHR-C: 42-week-old non-treated spontaneously hypertensive (SHR) rats, n=8; SHR-L: 42-week-old SHR rats that received L-2286 for 32 weeks, n=8. EF: ejection fraction, LVEDV: left ventricular end-diastolic volume, LVESV: left ventricular end-systolic volume. Septum: thickness of the septum, PW: thickness of the posterior wall, SBP: systolic blood pressure, HR: heart rate, VW/BW: ventricular weight to body weight ratio. The values are the means ± SEM. a $p<0.01$ vs. WKY, b $p<0.05$ vs. SHR-C.

3.2.2. The effect of L-2286 treatment on the size of mitochondria

The whole range of the mitochondrial areas that were found in cardiomyocytes was divided into seven equal ranges of 0.3 μm^2, in which the relative frequency of mitochondria was

determined. Fewer than 1% of the mitochondria were extremely large (areas greater than 2.1 μm^2) in each group of animals. In the WKY group, the most common range of the mitochondrial area was 0.3-0.6 μm^2 (Fig. 1A). In hypertensive control animals (Fig. 1B), approximately half of the measured mitochondria belonged to the lowest area range (<0.3 μm^2); however, in the WKY group, only appr. 20% of the mitochondria pertained to this area range. This result indicates a more fragmented phenotype of interfibrillar mitochondria due to hypertension-induced myocardial remodeling and oxidative stress. In L-2286-treated hypertensive animals, however, the distribution of the size of the mitochondria was similar to that in the WKY group, and most mitochondria belonged to the 0.3-0.6 μm^2 area range (Fig. 1C). Changes in mitochondrial size can also be assessed by determining the mean area or length of mitochondria in each group. Significantly lower values were detected in the SHR-C group compared to the normotensive group ($p<0.05$ SHR-C vs. WKY) (Fig. 1D). In terms of both the mean area and longitudinal axis of the mitochondria, a significant decrease was apparent in the SHR-C group ($p<0.01$, SHR-C vs. WKY) compared to the normotensive group (Fig. 1E). The worsening of these parameters was less pronounced in SHRs treated with L-2286 ($p<0.01$, SHR-L vs. SHR-C) (Fig. 1C, D, E).

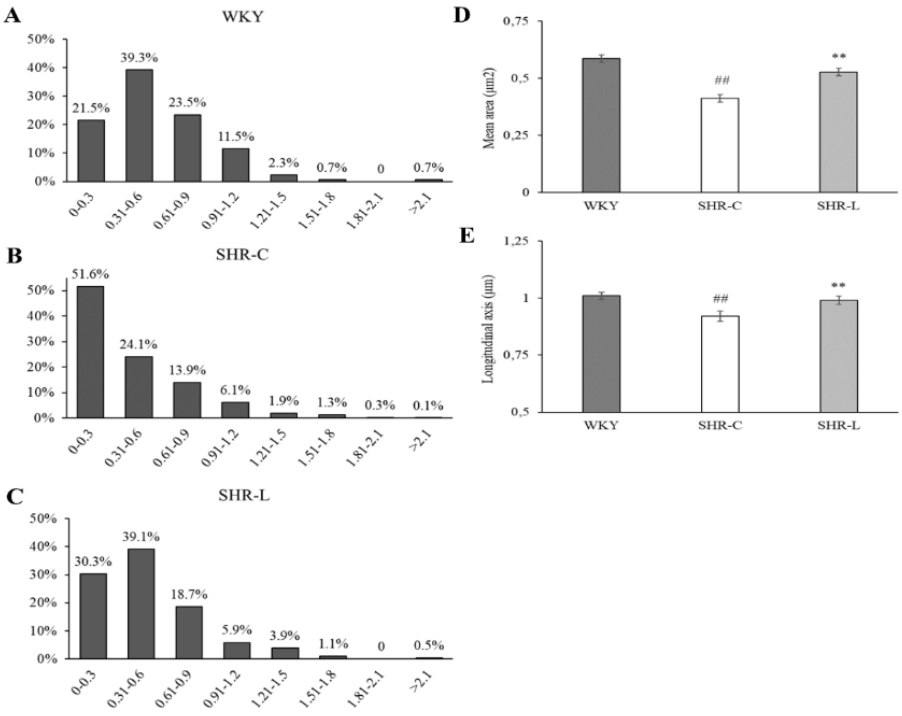

Figure 1. Hypertension-related fragmentation of interfibrillar mitochondria in the myocardium. *Distribution of mitochondria according to their size in various area range groups: (A) WKY: normotensive age-matched animals, (B) SHR-C: untreated spontaneously hypertensive (SHR) rats, (C) SHR-L: SHRs treated with L-2286. (D) Mean mitochondrial area. (E) Longitudinal axis of mitochondria. The values are presented as the means ± SEM ∗∗$p < 0.01$ vs. SHR-C, ##$p < 0.01$ vs. WKY.*

3.2.3. The effect of L-2286 treatment on the subcellular distribution of mitochondrial dynamics-related proteins

Opa1 was not detected in the cytosolic fraction. In mitochondrial fractions of SHR-C samples, the Opa1 level was decreased significantly compared to normotensive animals ($p < 0.01$, SHR-C vs. WKY). L-2286 treatment did not significantly influence the decrease of Opa1 levels in mitochondria (2A-C). Chronic hypertension-induced myocardial remodeling did not significantly affect the overall amount of the Drp1 protein in our animal model. Moreover, L-2286 treatment did not significantly alter the Drp1 protein level (data not shown). To assess the intracellular distribution of the Drp1 protein between the cytosolic and mitochondrial compartments, fractionated western blot samples were used.

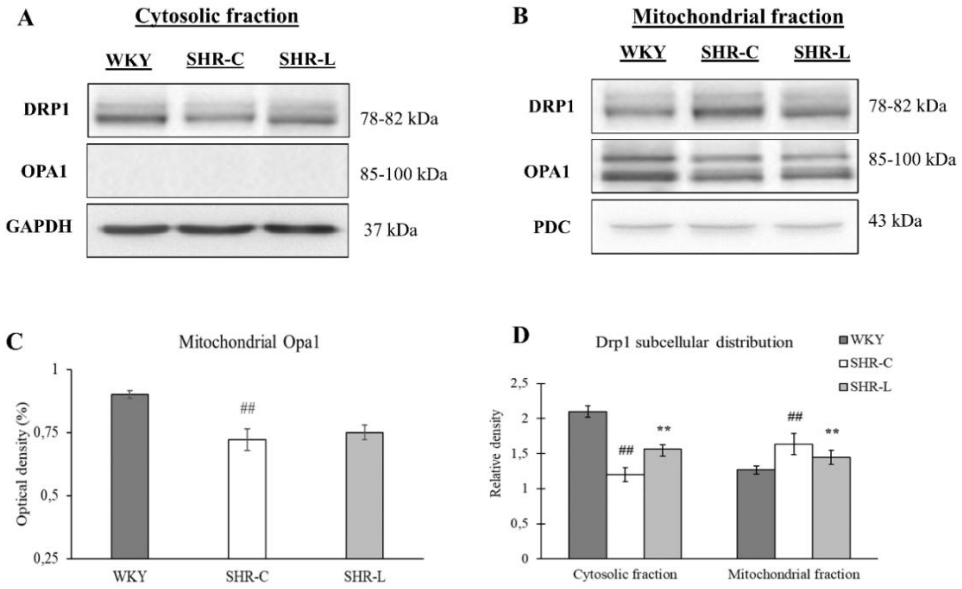

Figure 2. The effects of L-2286 treatment on the intracellular distribution of Drp1 and Opa1 proteins. *(A) Representative western blot analysis of Drp1 and Opa1 protein levels in the cytosolic fraction. (B) Representative western blot analysis of Drp1 and Opa1 protein levels in the mitochondrial fraction. GAPDH and PDC were used as loading controls. (C) Effects of L-2286 treatment on the mitochondrial fusion protein Opa1 in subcellular fractions. (D) Effects of L-2286 treatment on the cellular distribution of Drp1. SHR-C: non-treated spontaneously hypertensive (SHR) rats; SHR-L: SHRs treated with 5 mg/kg/day L-2286 for 32 weeks. The values are presented as the means ± SEM (n = 4), ##p < 0.01 vs. WKY, ∗p < 0.05 vs. SHR-C, ∗∗p < 0.01 vs. SHR-C.*

In the cytosolic fraction, the Drp1 level was the lowest in the non-treated hypertensive control group ($p < 0.01$, SHR-C vs. WKY) (2A, D). Inhibition of PARP-1 by L-2286 treatment retained a higher amount of Drp1 in the cytosol ($p < 0.01$ SHR-L vs. SHR-C). On the other hand, the greatest translocation of Drp1 into the mitochondria was observed in the SHR-C group ($p < 0.01$, SHR-C vs. WKY) (2B, D). L-2286 treatment reduced the level of Drp1 in the mitochondrial fraction ($p < 0.05$, SHR-L vs. SHR-C).

3.2.4. The effects of L-2286 treatment on glutathione levels and auto-PARylation in NRCMs

During oxidative stress, the level of GSH decreases; thus, the GSH/GSSG ratio also decreases. In our experiments, H_2O_2 induced a significant decrease in the GSH level in NRCMs, indicating oxidative damage. L-2286 treatment, on the other hand, ameliorated this detrimental effect of oxidative stress. To detect the effectiveness of L-2286 treatment, the activity of ADP-ribosylation processes in NRCM cell samples was analyzed via capillary western blotting. The most pronounced auto-PARylation was observed in the H_2O_2 group; however, L-2286 treatment alleviated this unfavorable effect.

3.2.5. Morphological changes in the mitochondrial network

In control NRCMs, the mitochondrial reticulum was normal with a long, regular shape. However, oxidative stress induced marked morphological changes, the mitochondrial network became fragmented, and consequently, small, dot-like mitochondria could be observed. L-2286 treatment protected the mitochondrial network against oxidative stress-induced damage in NRCMs; therefore, the mitochondrial network remained reticular, similar to that in the control cells.

3.2.6. Effects of L-2286 on the cellular level and subcellular distribution of fission-fusion regulator proteins

Our data revealed that L-2286 treatment significantly increased the amount of the mitochondrial fusion proteins Mfn2 and Opa1 compared with that in the stressed group and the control group ($p<0.01$ H_2O_2+L-2286 vs. H_2O_2 and vs. Control), but no significant change in the expression level of the Mfn1 protein was detected. In response to L-2286 treatment, the levels of the mitochondrial fission proteins Drp1 ($p<0.05$) and Fis1 ($p<0.01$) were markedly decreased than those in the stressed group, where these values were the highest ($p<0.01$ H_2O_2 vs. control). We also examined the phosphorylation state of the Drp1 protein because the phosphorylation of Drp1 at Serine 616 residues promotes mitochondrial fission; however, the phosphorylation of the Drp1 at Serine 637 residue inhibits enzyme activity and its translocation into the mitochondria. We demonstrated that L-2286 treatment significantly decreased the phosphorylation state of Drp1 at Serine 616 residues ($p<0.01$, H_2O_2+L-2286 vs. H_2O_2 group); moreover, PARP-inhibition considerably increased the phosphorylation state of Drp1 at Serine 637 residue compared to stressed group ($p<0.01$,

H_2O_2+L-2286 vs. H_2O_2). However, in the mitochondrial fraction of L-2286-treated stressed cells, the level of Opa1 increased significantly compared to stressed only group ($p<0.01$, H_2O_2+L-2286 vs. H_2O_2). The amount of cytosolic Drp1 in the stressed only group (H_2O_2) was the lowest. Inhibition of PARP-1 by L-2286 treatment resulted in a significantly greater amount of Drp1 remaining in the cytosol ($p<0.01$ H_2O_2+L-2286 vs. H_2O_2). Therefore, intracellular Drp1 localization was strongly influenced by PARP-inhibition because the level of the Drp1 protein was significantly lower in the mitochondrial fraction and higher in the cytosolic fraction of treated cells compared to stressed only NRCM cells ($p<0.01$, H_2O_2+L-2286 vs. H_2O_2).

3.2.7. Examination of mitochondrial function via the membrane potential and oxygen consumption rate

We examined the effect of PARP-inhibition on the mitochondrial membrane potential using JC-1, a cell-permeable, voltage-sensitive, fluorescent mitochondrial dye. Fluorescent microscopy revealed strong red and weak green fluorescence in the control group, which indicates normal, healthy mitochondrial membrane potential (high ΔΨm). The mitochondrial membrane depolarizes in response to H_2O_2 stress, resulting in weaker red and stronger green fluorescence.

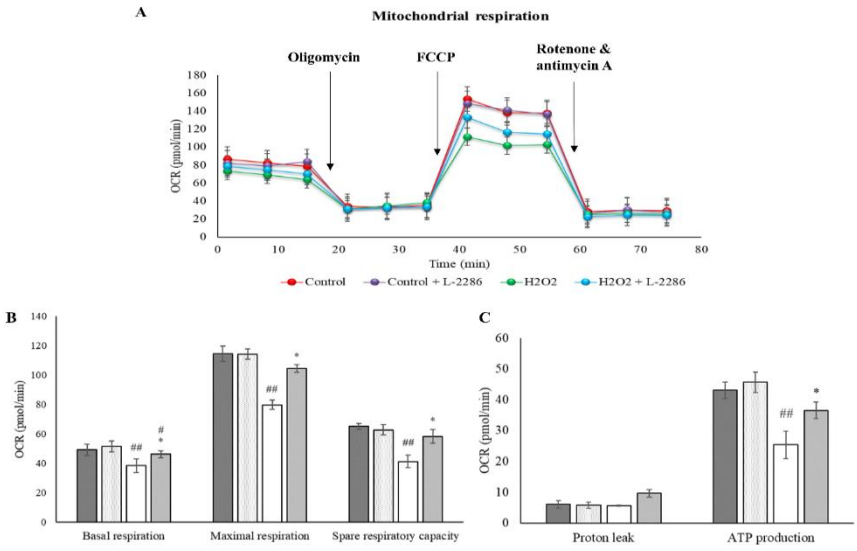

Figure 3. The effect of L-2286 treatment on the oxygen consumption rate in NRCM cells. *(A) The oxygen consumption rate (OCR) in NRCMs was measured with a Seahorse XFp Analyzer. (B) Basal respiration, maximal respiration and spare respiratory capacity of NRCMs. (C) Proton leak and ATP production ability of NRCMs. The groups of cells were as follows: Control: cells without any treatment; Control+L-2286: cells incubated with 10 μM L-2286 for 0.5 hours; H_2O_2: cells stressed with 150 μM H_2O_2 for 0.5 hours; H_2O_2+L-2286: cells stressed with 150 μM H_2O_2 and treated with 10 μM L-2286 for 0.5 hours. The values are the means ± SEM (n=4). ##p<0.01 vs. the Control group; #p<0.05 vs. the Control group; *p<0.05 vs. the H_2O_2 group.*

When L-2286 was added to hydrogen-peroxide stressed cells, the decrease in the mitochondrial membrane potential was smaller; therefore, the red and green fluorescence values were similar to those of the control cells. By quantifying these changes, we observed that the mitochondrial membrane potential was reduced due to oxidative stress ($p<0.05$, H_2O_2 vs. Control), and this unfavorable change was moderated by L-2286 treatment in our cell culture model ($p<0.05$, H_2O_2+L-2286 vs. H_2O_2). To determine mitochondrial energy metabolism and respiratory function, we used the Agilent Seahorse XFp Analyser system and the Agilent Seahorse XFp Cell Mito Stress Test (Fig. 3A and B). L-2286 itself had no effect on the rate of mitochondrial respiration. However, we observed that (Fig. 3A) H_2O_2 treatment decreased basal respiration, maximal respiration, spare respiratory capacity and ATP production as a result of H_2O_2-induced oxidative damage compared with those of the Control group ($p<0.01$, H_2O_2 vs. Control). Due to L-2286 treatment, the spare respiratory capacity, which is a measure of the ability of cells to respond to increased energy demand or under stress, and ATP production ability increased significantly ($p<0.05$, H_2O_2+L-2286 vs. H_2O_2).

3.2.8. The effect of L-2286 treatment on mitochondrial biogenesis

L-2286 treatment enhanced mitochondrial biogenesis and function in stressed NRCMs. While no differences were observed in non-stressed cells, L-2286 significantly increased PGC-1α expression ($p<0.01$) and CREB phosphorylation at Ser133 ($p<0.01$) under oxidative stress. Hydrogen-peroxide reduced mitochondrial content, as indicated by decreased VDAC levels ($p<0.05$), but L-2286 restored and even increased VDAC levels beyond control values ($p<0.01$). Respiratory chain proteins NDUFs1 and UQCRC1 were also reduced by oxidative stress ($p<0.01$), but L-2286 treatment prevented this decline ($p<0.01$). Mitochondrial DNA content (COX1, COX3) and citrate synthase activity were also elevated with L-2286, further supporting its role in mitochondrial biogenesis.

3.2.9. The effect of L-2286 treatment on mitochondrial genome integrity

In the present study, we used H_2O_2 as a toxic agent with the potential to damage DNA. Using real-time detection of long-range PCR (14958 bp; LRPCR) and short-range PCR (210 bp; SRPCR), we examined the impact of 150 μM H_2O_2 on mtDNA integrity. These data show

that oxidative stress induced significant damage to mtDNA in the stressed group ($p<0.01$ vs. Control group). Compared with that in the stressed group, the amount of mitochondrial DNA in the treated group was less fragmented, and the relative expression level of mitochondrial DNA was markedly increased (approximately 4-fold) ($p<0.01$, H_2O_2+L-2286 vs. H_2O_2) (Fig. 4.).

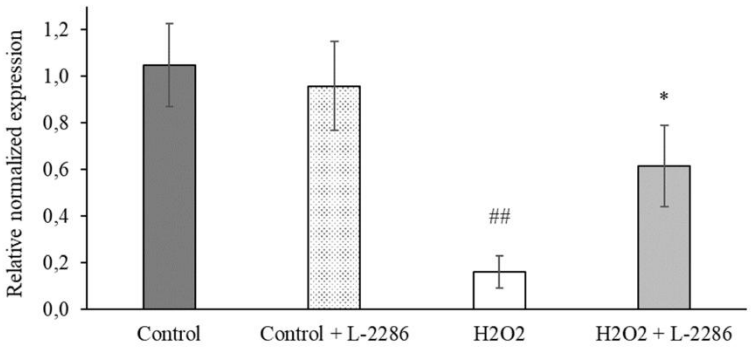

Figure 4. Effect of L-2286 treatment on oxidative stress-induced mitochondrial DNA damage. *After the appropriate treatment, total DNA was isolated for LRPCR and SRPCR analysis as indicated in the Methods section. mtDNA damage was calculated via the Δ2Ct method. Control group: cells without any treatment; Control + L-2286 group: cells treated with only 10 μM L-2286 for 0.5 hours; H_2O_2 group: cells treated with 150 μM H_2O_2 for 0.5 hours; H_2O_2 + L-2286 group: cells treated with 150 μM H_2O_2 and 10 μM L-2286 for 0.5 hours. The values are presented as the means ± SEM (n=4), ##p<0.01 vs. the Control group, *p<0.05 vs. the H_2O_2 group.*

4. THE EFFECT OF COLCHICINE TREATMENT ON PULMONARY ARTERIAL HYPERTENSION

4.1. METHODS

4.1.1. Animal model

Eight-week-old male Wistar Kyoto rats (WKY) were purchased from Janvier-Labs (Marseille, France) and were kept as described previously. WKY rats were randomized into four groups: a single subcutaneous injection of 60 mg/kg monocrotaline was administered to 8-week-old male Wistar rats (n=20) to induce PAH. Fourteen days after the MCT injection, the MCT+C group was treated with an intraperitoneal injection of 0.5 mg/kg colchicine three times a week for 2 weeks. There were two additional control groups: the third group received only physiological saline without MCT and colchicine (CONT), and the fourth group received 0.5 mg/kg colchicine three times per week, starting from the same day as the second group but without MCT pretreatment (CONT+C). The rats were inspected daily to measure their weight and to observe their normal activity, respiration, responsiveness to manipulations and general characteristics. At the end of the study, the animals were euthanized with an overdose of isoflurane, and the organs were harvested.

4.1.2. Experimental protocol

All animals were examined with echocardiography to exclude rats with any heart abnormalities. Transthoracic two-dimensional echocardiography was performed under inhalation anesthesia. Cardiac dimensions and function were measured from short- and long-axis views at the mid-papillary level by a VEVO 3100 high-resolution ultrasound imaging system (VisualSonics, Toronto, Canada) equipped with a 25 MHz transducer. The ejection fraction (EF%), LV end-diastolic internal diameter (LVIDd), LV end-systolic internal diameter (LVIDs), E/A and E/e' ratios, tricuspid annular plane systolic excursion (TAPSE) and pulmonary arterial acceleration time (PAT) were determined. At the end of the study, the animals were euthanized with an overdose of isoflurane, and the hearts and lungs were removed for histological processing or western blot analysis. We examined cardiac remodeling-related signaling pathways in the RV using Western blot (MAPKs, TGFβ-Smad, prosurvival factors). We evaluated the effect of colchicine treatment on the metabolic and inflammatory profile of the right ventricle (LDH, PDH, mitochondrial enzyme activity).

4.2. RESULTS

4.2.1. Effect of colchicine on the lung vasculature

The effect of colchicine on pulmonary vascular remodeling was examined in hematoxylin–eosin-stained sections. An analysis of the small pulmonary arteries (100-250 μm in diameter) revealed that the WA% and WT% in the MCT group were significantly greater than those in the control group ($p<0.01$). The colchicine treatment alleviated this detrimental effect of PAH ($p<0.01$). The muscularization of pulmonary arterioles was assessed with immunohistochemistry targeting the smooth muscle cell marker α-SMA. The α-SMA expression was increased in the MCT group compared to the CONT group ($p<0.01$). This phenomenon was significantly attenuated by colchicine treatment ($p<0.01$). Statistical analysis revealed a noteworthy reduction in the proportion of fully muscularized pulmonary arteries due to colchicine treatment ($p<0.01$). MCT treatment caused a significant increase in the collagen content in the wall of the lung vessels ($p<0.01$), which was reversed by colchicine treatment ($p<0.01$).

4.2.2. Effect of colchicine on echocardiographic and gravimetric parameters

Table 2. *Effect of colchicine treatment on echocardiographic and gravimetric parameters.*

	CONT	CONT+C	MCT	MCT+C
LVIDd (mm)	6.424 ± 0.27	6.649 ± 0.21	6.328 ± 0.49	6.285 ± 0.21
LVIDs (mm)	3.151 ± 0.18	3.668 ± 0.15	3.412 ± 0.51	3.184 ± 0.21
EF (%)	82.45 ± 1.97	77.74 ± 1.89	79.93 ± 3.35	82.13 ± 2.33
E/A	1.681 ± 0.09	2.061 ± 0.32	1.449 ± 0.11	1.886 ± 0.11
E/e'	23.77 ± 2.94	23.92 ± 1.82	19.55 ± 1.42	22.06 ± 1.83
TAPSE (mm)	1.947 ± 0.15	2.086 ± 0.13	1.186 ± 0.08*	1.773 ± 0.09$^{\$}$
PAT (ms)	21.25 ± 1.86	22.73 ± 1.75	18.52 ± 0.76*	22.82 ± 0.91$^{\$}$
VW/BW (mg/g)	3.004 ± 0.08	3.1 ± 0.038	3.517 ± 0.061**	3.19 ± 0.047$^{\$\$}$
VW/Tibia (mg/mm)	20.22 ± 0.77	18.92 ± 0.64	23.28 ± 0.59**	19.19 ± 0.65$^{\$\$}$
Lung wet weight/dry weight (mg/mg)	4.77 ± 0.045	4.8 ± 0.115	4.83 ± 0.054	4.76 ± 0.222

*CONT: control group, CONT+C: control group treated with colchicine for 2 weeks, MCT: group received 60 mg/kg monocrotaline, MCT+C: monocrotaline pretreatment and colchicine treatment for 2 weeks, n=10. LVIDs: left-ventricular internal diameter end-systolic; LVIDd: left-ventricular internal diameter end-diastolic; EF: ejection fraction, E: mitral peak velocity of early filling; A: mitral peak velocity of late filling; e': early diastolic mitral annular velocity; TAPSE: tricuspid annular plane systolic excursion; PAT: pulmonary arterial acceleration time; VW: ventricular weight; BW: body weight; Tibia: length of right tibia. Values are means ± SEM * p<0.05 CONT vs. MCT; $ p<0.05 MCT vs. MCT+C;** p<0.01 CONT vs. MCT; $$ p<0.01 MCT vs. MCT+C*

4.2.3. Effect of colchicine on cardiac interstitial collagen deposition and cardiomyocyte diameter

To detect the effect of colchicine treatment on interstitial collagen deposition, paraffin-embedded right ventricular sections were stained with Picrosirius red (Fig. 5.). In the CONT and CONT+C groups, only a small amount of interstitial fibrosis was observed. High blood pressure in the lung causes a marked increase in collagen deposition in the heart. The extent of fibrosis was significantly greater in the MCT group than in the CONT group ($p<0.01$). The administration of colchicine to MCT-pretreated rats resulted in a significantly lower collagen extent ($p<0.01$). In addition, histological samples from the right ventricle stained with Picrosirius red were used to measure the cell diameters. The most pronounced increase in cell diameter was detected in the MCT group. The average cell diameter was 32.2 ± 1.97 µm in the MCT group, whereas in the CONT group, this value was only 20.99 ± 1.36 µm ($p<0.01$). The colchicine treatment resulted in significantly smaller cell diameters (25.66 ± 1.46 µm) in the MCT+C group compared to the MCT group ($p<0.01$).

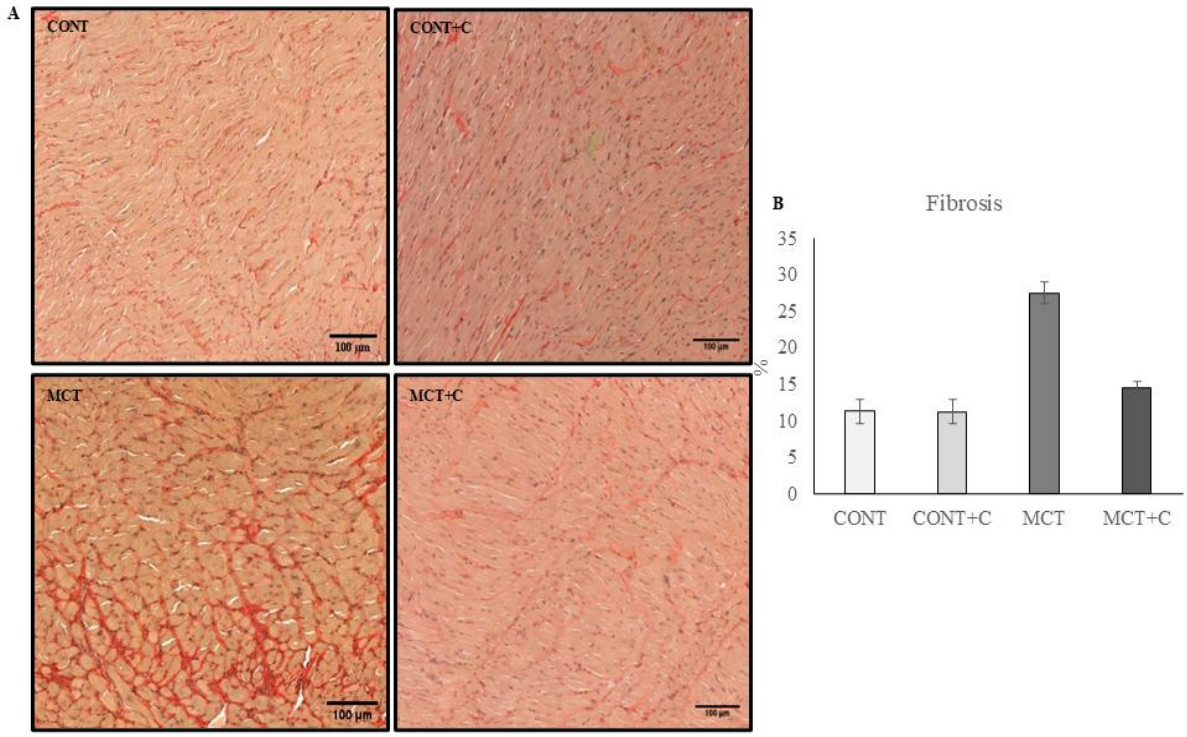

Figure 5. Colchicine treatment decreases the extent of interstitial collagen deposition in the right ventricle and the degree of cardiac hypertrophy. *(A) Representative histological sections stained with Picrosirius red (n=5). Scale bar: 100 µm; magnification: 10×. (B) A densitometric evaluation of the sections is shown. The values are the means ± SEMs (n=5). ** p<0.01 CONT vs. MCT; $$ p<0.01 MCT vs. MCT+C.*

4.1.3. Effect of colchicine on signaling pathways in the right ventricle

Colchicine treatment mitigated fibrosis-related signaling in the MCT+C group. TGF-β expression was significantly elevated in MCT compared to controls ($p<0.05$) but was reduced following colchicine treatment ($p<0.05$). The phosphorylation of Smad2 and Smad3, key downstream effectors of TGF-β, was increased in MCT, with colchicine significantly decreasing Smad2 activation ($p<0.05$) and markedly reducing Smad3 phosphorylation ($p<0.01$). The phosphorylation levels of p38-MAPK and JNK were highest in the MCT group ($p<0.01$), while colchicine treatment led to a significant reduction in their activation ($p<0.05$). In contrast, MKP-1, an upstream regulator of MAPKs, was significantly elevated in MCT compared to controls ($p<0.01$) and further increased with colchicine ($p<0.01$), suggesting a regulatory feedback mechanism. ERK1/2 and Akt1 phosphorylation levels were low in controls and the MCT group but were significantly increased following colchicine treatment ($p<0.01$). Similarly, GSK-3β phosphorylation, which was low in controls and MCT, was highest in the colchicine-treated MCT group ($p<0.01$).

4.1.4. Effect of colchicine treatment on enzyme activities in the right ventricle

A mitochondrial metabolic abnormality can be observed in PAH cases. This represents a glycolytic shift, which results in anaerobic glycolysis due to the inhibition of the pyruvate-dehydrogenase enzyme. This glycolytic shift in RV myocytes contributes to a reduction in myocardial contractility. To assess the effectiveness of colchicine treatment, pyruvate-dehydrogenase and lactate dehydrogenase enzyme activity was analyzed in right ventricular tissue. Pyruvate-dehydrogenase (PDH) activity, which was slightly reduced in the MCT group, significantly increased with colchicine treatment ($p<0.01$, MCT+C vs. MCT), while lactate-dehydrogenase (LDH) activity, elevated in MCT ($p<0.01$), showed a non-significant decrease with colchicine. One of the key principles of cellular energy production is the link between cytosolic glycolysis and the mitochondrial Krebs cycle, where pyruvate serves as a substrate and leads to the production of reduced coenzymes (NADH and $FADH_2$), which provide electrons to the mitochondrial electron transport chain (ETC). To assess the effectiveness of colchicine treatment, the enzyme activity of NADH:cytochrome C oxidoreductase, and citrate-synthase were analyzed in right ventricular tissue. NADH:cytochrome C oxidoreductase activity is essentially the combined reaction of ETC complex I and complex III, with ubiquinone acting as the transporter of hydrogen between the 2 complexes. NADH:cytochrome C oxidoreductase activity was slightly but

significantly reduced in MCT ($p<0.05$) and restored with colchicine ($p<0.05$). Citrate synthase activity, in MCT tended to decrease, but this difference was not statistically significant. However, the administration of colchicine significantly increased citrate synthase enzyme activity in the MCT-treated group ($p<0.01$).

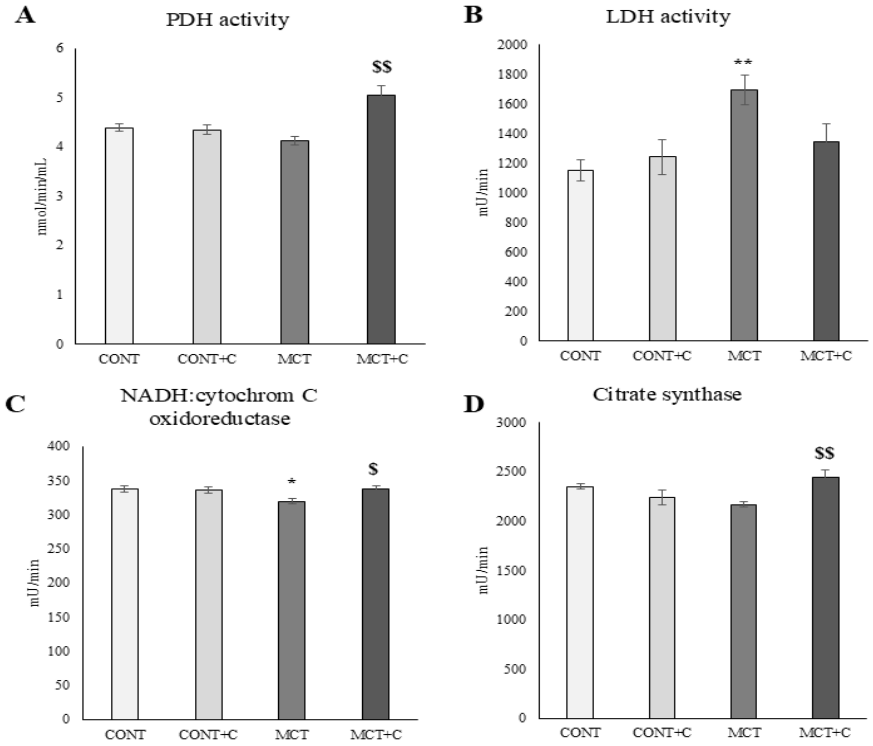

Figure 6. Effect of colchicine treatment enzyme activities. *(A) Colchicine treatment enhances PDH enzyme activity. (B) Effects of colchicine administration on LDH enzyme activity. Colchicine treatment improves NADH:cytochrome C oxidoreductase (C) and citrate synthase (D) enzyme activity in RV myocytes. The bar diagrams represent the means ± SEM (n=8). $$ p<0.01 MCT vs. MCT+C; ** p<0.01 CONT vs. MCT.*

4.1.5. The effects of colchicine on cytokine and chemokine expression

Thymus chemokine (CXCL7), sICAM-1, and L-selectin play a role in inflammatory processes, leukocyte recruitment, and leukocyte-endothelial interactions. MCT treatment significantly increased the levels of CXCL7, sICAM-1, and L-selectin ($p<0.01$ vs. CONT). Our results revealed an increased level of VEGF-A in the MCT group ($p<0.01$ MCT vs. CONT), which was decreased by colchicine treatment in the MCT+C group ($p<0.01$ MCT+C vs. MCT). Since the histopathological sections revealed fibrosis upon MCT treatment, we investigated the expression level of TIMP-1. Our results showed elevated levels of TIMP-1 in the MCT group ($p<0.01$ MCT vs. CONT). However, colchicine treatment caused a significant decrease in the level of TIMP-1 in the MCT+C group ($p<0.01$ MCT+C vs. MCT).

5. DISCUSSION

The first study demonstrated that pharmacological PARP inhibition protects against hypertensive heart disease by preserving mitochondrial structure and function. Using the SHR model, we observed that untreated hypertensive animals developed left ventricular hypertrophy without overt heart failure symptoms. Untreated SHRs exhibited increased left ventricular mass and wall thickness, accompanied by mitochondrial fragmentation, cristae disruption, and altered mitochondrial dynamics. PARP inhibition reduced cardiac hypertrophy and prevented mitochondrial dysfunction by blocking Drp1-mediated fission and preserving mitochondrial fusion (Opa1, Mfn2). In vitro, oxidative stress induced by hydrogen peroxide led to PARP activation, mitochondrial fragmentation, and impaired respiratory capacity in neonatal cardiomyocytes. PARP inhibition prevented these changes by enhancing mitochondrial biogenesis via PGC-1α activation and reducing oxidative stress markers. Additionally, it preserved mtDNA integrity, mitochondrial enzyme activity, and ATP production, improving cellular energy metabolism. These findings suggest that PARP inhibition counteracts mitochondrial dysfunction and hypertrophic remodeling in hypertensive heart disease.

The second study showed that colchicine treatment prevents right ventricular failure in pulmonary arterial hypertension by mitigating inflammation, metabolic dysfunction, and structural remodeling. In the MCT-induced PAH model, colchicine significantly reduced pulmonary vascular remodeling, as indicated by decreased smooth muscle cell proliferation and collagen deposition. It also attenuated RV hypertrophy and fibrosis by lowering cardiomyocyte diameter and interstitial collagen accumulation. Echocardiographic findings revealed colchicine improved RV function by increasing PAT and TAPSE, suggesting enhanced contractility and adaptation to increased afterload. At the molecular level, colchicine reduced pro-fibrotic and inflammatory signaling pathways (TGF-β/Smad, JNK, p38-MAPK) while enhancing prosurvival and metabolic pathways (ERK1/2, Akt1, GSK-3β). Metabolically, colchicine treatment restored mitochondrial function by increasing PDH activity and reducing LDH activity, thereby reversing the glycolytic shift characteristic of PAH. It also enhanced oxidative phosphorylation by restoring citrate synthase and NADH:cytochrome C oxidoreductase activity, leading to improved mitochondrial energy production. Furthermore, colchicine significantly decreased the levels of inflammatory mediators such as CXCL7, sICAM-1, and VEGF-A, indicating an overall anti-inflammatory effect that contributed to its cardioprotective role.

6. SUMMARY OF THE NEW FINDINGS

1. **The PARP-inhibition had a beneficial effect on LV hypertrophy.**

   We demonstrated that L-2286 treatment has beneficial effects on cardiac function in hypertension-induced heart failure, especially in the context of LV hypertrophy.

2. **In the SHR model, the L-2286 treatment positively affected the morphology and size distribution of IFM.**

   L-2286 treatment prevented hypertension-induced mitochondrial damage. L-2286 had a beneficial effect on mitochondrial morphology and the subcellular distribution of mitochondrial dynamics-related proteins in hypertension-induced heart failure.

3. **The L-2286 preserved the physiological mitochondrial structure and function in an oxidative-stressed NRCM model.**

   L-2286 treatment preserved mitochondrial morphology and function. Under oxidative stress conditions, physiological mitochondrial membrane potential is maintained, and mitochondrial respiratory function is improved.

4. **The L-2286 treatment enhanced mitochondrial quality control processes in stressed cardiomyocytes.**

   L-2286 treatment increased the expression level of fusion proteins (Opa1 and Mfn2) and decreased the level of fission proteins (Drp1 and Fis1). It enhances mitochondrial biogenesis through the PGC-1α-CREB pathway. L-2286 treatment protected against oxidative stress-induced mtDNA damage by maintaining genome integrity.

5. **Colchicine treatment protected against pulmonary arterial remodeling and improved RV function.**

   We verified that short-term low-dose colchicine treatment has beneficial effects on cardiac function, especially RV function, in the MCT-induced PAH model. Besides this, colchicine treatment also has a positive impact on pulmonary arterial remodeling.

6. **Colchicine treatment positively influenced the signaling pathways in the RV.**

   Colchicine treatment positively influences the activity of signaling pathways involved in cardiac remodeling (JNK, p38 MAPK, ERK1/2, and Akt1-GSK-3β).

7. **Administration of colchicine had beneficial effects on the metabolic and inflammatory profile of the RV.**

   Colchicine treatment prevents chronic inflammation in the RV by decreasing pro-inflammatory cytokines and adhesion molecules. In addition, colchicine treatment protects physiological energy metabolism in the RV during PAH by increasing the activity of PDH and enhancing the oxidative phosphorylation capacity.

7. ACKNOWLEDGEMENT

These studies were carried out at the 1st Department of Medicine, at the Szentágothai Research Centre and at the Department of Biochemistry and Medical Chemistry, Medical School of the University of Pécs, between 2020 and 2024.

I would like to express my sincere gratitude to my former Program Leader, **Professor Kálmán Tóth**, and my current Program Leader, **Professor Ferenc Gallyas**, for their support and guidance throughout my work.

I would like to express my heartfelt gratitude to my project leader, **Professor Róbert Halmosi** and to **Dr. László Deres**, for their mentorship in the field of cardiovascular sciences and for providing the opportunity to carry out this work. Without their essential guidance and intense support, this dissertation would not have been possible.

I am thankful to all my present and former colleagues, especially **Dr. Krisztián Erős, Dr. Orsolya Horváth, Dr. Szilárd Tóth** and **Dr. Krisztina Fekete**, for their contributions and helping hands in the experiments.

I am truly grateful to **Tímea Dózsa** and **József Nyirádi**, who provided invaluable assistance with laboratory work and histological processing during my studies.

I would like to extend my heartfelt thanks to **my close friends**, who were always there to cheer me on and remind me of the importance of taking a step back and finding balance. Their belief in me has been a source of great motivation.

I am profoundly grateful to **my family**, whose unwavering support has been the foundation of my journey. Their encouragement, love, and understanding provided me with the strength to persevere through the challenges of this project.

Above all, I owe my deepest gratitude to **my husband**, whose constant support, patience, and love have been my anchor. His belief in me, even during moments of doubt, has been instrumental in completing this dissertation. Thank you for being my greatest source of strength and inspiration.

8. PUBLICATIONS OF THE AUTHOR

Relevant publication

ORDOG K, HORVATH O, EROS K, BRUSZT K, TOTH SZ, KOVACS D, KALMAN N, RADNAI B, DERES L, GALLYAS F, TOTH K, HALMOSI R. Mitochondrial protective effects of PARP-inhibition in hypertension-induced myocardial remodeling and in stressed cardiomyocytes. Life Sciences 268 Paper: 118936, 15 p. (2021) **IF: 6.78; Q1, D1**

ORDOG K, HORVATH O, TOTH SZ, DERES L, KOVACS K, SOOS SZ, GALLYAS F, TOTH K, HALMOSI R, CZOPF L. Colchicine as a therapeutic possibility for the treatment of pulmonary arterial hypertension (PAH) in a rat model. ***(under publication; IF: 5.3; Q1*** *Biochemical Pharmacology)*

Additional publications

BRUSZT K, HORVATH O, **ORDOG K**, TOTH SZ, JUHASZ K, VAMOS E, FEKETE K, GALLYAS F, TOTH K, HALMOSI R, DERES L. Cardiac effect of OPA1 protein promotion in a transgenic animal model. Plos One 2024;19(11):e0310394. (2024); **IF: 2.9; Q1**

HORVATH O, **ORDOG K**, BRUSZT K, DERES L, GALLYAS F, SUMEGI B, TOTH K, HALMOSI R. BGP-15 protects against heart failure by enhanced mitochondrial biogenesis and decreased fibrotic remodelling in spontaneously hypertensive rats. Oxidative Medicine and Cellular Longevity 2021 Paper: 1250858, 13 p. (2021); **IF: 7.31; Q1**

PAKAI E, TEKUS V, ZSIBORAS CS, RUMBUS Z, OLAH E, KERINGER P, KHIDHIR N, MATICS R, DERES L, **ORDOG K**, SZENTES N, POHOCZKY K, KEMENY A, HEGYI P, PINTER E, GARAMI A. The neurokinin-1 receptor contributes to early phase of lipopolysaccharide-induced fever via stimulation of peripheral cyclooxygenase-e protein expression in mice. Frontiers in Immunology 2018 Paper: 166. 15 p (2018); **IF: 4.716; Q1**

BOGDAN M, PERIC L, **ORDOG K**, VUKOVIC D, URBAN E, SOKI J. The first characterized carbapenem-resistant Bacteriodes fragilis strain from Croatia and the case study for it. Acta Microbiologica et Immunologica Hungarica 65:3 pp. 317-323, 7p, (2018). **IF: 1.079; Q3**

Cumulative impact factor: 28.085

Published Abstracts

ORDOG K, HORVATH O, TOTH SZ, FEKETE K, GALLYAS F, KOVACS K, DERES L, TOTH K, HALMOSI R, CZOPF L. Colchicine as a therapeutic option for the treatment of pulmonary arterial hypertension (PAH) in a rat model. EUROPEAN HEART JOURNAL 45: Suppl. 1 ehae666.3702 (2024)

ORDOG K, HORVATH O, TOTH SZ, FEKETE K, GALLYAS F, KOVACS K, TOTH K, DERES L, HALMOSI R, CZOPF L. Colchicine as a novel therapeutic option for the treatment of pulmonary arterial hypertension (PAH) in a rat model. CARDIOLOGIA HUNGARICA Supplementum C, C332 (2024)

TOTH SZ, SALAME E, FEKET K, **ORDOG K**, HORVATH O, TOTH K, HALMOSI R, DERES L. Effect of isoflurane anesthesia on echocardiographic parameters in mice. CARDIOLOGIA HUNGARICA Supplementum C, C265 (2024)

BRUSZT K, HORVATH O, **ORDOG K**, TOTH SZ, VAMOS E, JUHASZ K, TOTH K, DERES L, HALMOSI R. The effects of levosimendan and its active metabolite on mitochondrial function. CARDIOLOGIA HUNGARICA Supplementum C, C260 (2024)

BRUSZT K, HORVATH O, **ORDOG K**, TOTH SZ, VAMOS E, GALLYAS F, TOTH K, DERES L, HALMOSI R. Effect of conventional and new types of positive inotropic agents on mitochondrial respiration. CARDIOLOGIA HUNGARICA Supplementum A, A279 (2023)

HORVATH O, **ORDOG K**, BRUSZT K, TOTH SZ, DERES L, GALLYAS F, TOTH K, SOOS SZ, HALMOSI R. The effect of BGP-15 treatment on heart function in a bleomycin-induced right-sided heart failure model. CARDIOLOGIA HUNGARICA Supplementum A, A301, (2023)

ORDOG K, HORVATH O, TOTH SZ, BRUSZT K, HABON T, KOVACS K, GALLYAS F, TOTH K, DERES L, HALMOSI R, CZOPF L. Effect of colchicine treatment on pulmonary arterial hypertension in a rat model. CARDIOLOGIA HUNGARICA Supplementum A, A303 (2023)

ORDOG K, HORVATH O, TOTH SZ, BRUSZT K, HABON T, KOVACS K, GALLYAS F, TOTH K, DERES L, HALMOSI R, CZOPF L. Investigating the effect of colchicine treatment on pulmonary arterial hypertension in a rat model. EUROPEAN JOURNAL OF HEART FAILURE 25: Suppl. S2. 439. (2023)

DERES L, **ORDOG K**, HORVATH O, BRUSZT K, TOTH SZ, GALLYAS F, TOTH K, HALMOSI R. Characterization of cardiac effects of OPA1 protein promotion in transgenic animal model. European Heart Journal, Volume 43, Issue Supplement_2, (2022)

BRUSZT K, HORVATH O, **ORDOG K**, TOTH SZ, FEKETE K, VAMOS E, TOTH K, DERES L, HALMOSI R. Effect of dopamine and dobutamine on the efficiency of mitochondrial respiration in cardiomyocytes. CARDIOLOGIA HUNGARICA Supplementum C, C253 (2022)

TOTH SZ, **ORDOG K**, HORVATH O, BRUSZT K, FEKETE K, GALLYAS F, TOTH K, HALMOSI R, DERES L. The effect of OPA1 promotion on mitochondrial dynamics in a transgenic animal model. CARDIOLOGIA HUNGARICA Supplementum C, C261 (2022)

ORDOG K, HORVATH O, BRUSZT K, HABON T, KALAI T, DERES L, TOTH K, HALMOSI R. The effect of PARP-inhibition on mitochondrial biogenesis in in vitro cardiomyocytes model. CARDIOLOGIA HUNGARICA Supplementum B, B244 (2021)

DERES L, TOTH SZ, BRUSZT K, **ORDOG K**, HORVATH O, GALLYAS F, TOTH K, HALMOSI R. The characterization of cardiac effect of OPA1 protein promotion in transgenic animal model. CARDIOLOGIA HUNGARICA Supplementum B, B274 (2021)

HORVATH O, **ORDOG K**, BRUSZT K, DERES L, GALLYAS F, TOTH K, HALMOSI R. Role of BGP-15 treatment on mitochondrial quality-control processes in an in vivo hypertension-induced heart failure model. CARDIOLOGIA HUNGARICA Supplementum D, D161 (2020)

ORDOG K, HORVATH O, BRUSZT K, HALMOSI R, TOTH K, SUMEGI B, DERES L. The effect of L-2286 treatment in oxidative stress on mitochondrial dynamics and function in an in vitro cardiomyoblast model. CARDIOLOGIA HUNGARICA Supplementum B, B14 (2019)

HOVATH O, **ORDOG K**, BRUSZT K, DERES L, SUMEGI B, TOTH K, HALMOSI R. The effect of BGP-15 treatment on mitochondrial dynamics and function in in vivo animal model and in cell culture. CARDIOLOGIA HUNGARICA Supplementum B, B23 (2019)

HORVATH O, DERES L, **ORDOG K**, BRUSZT K, SUMEGI B, TOTH K, HALMOSI R. Role of BGP-15 treatment in hypertensive heart failure Progression and mitochondrial protection. EUROPEAN HEART JOURNAL 40: Suppl. 1 Paper: P5994 (2019)

HORVATH O, DERES L, EROS K, **ORDOG K**, HABON T, SUMEGI B, TOTH K, HALMOSI R. Oxidative stress-induced changes in mitochondrial dynamics of cardiomyocytes in cell culture. EUROPEAN JOURNAL OF HEART FAILURE 20: Suppl. 1 pp. 616-616. Paper: P2281, 1p. (2018)

ORDOG K, DERES L, EROS K, HORVATH O, HABON T, SUMEGI B, TOTH K, HALMOSI R. Effect of BGP-15 treatment on hypertension induced cardiac remodeling in an in vivo SHR model. EUROPEAN JOURNAL OF HEART FAILURE 20: Suppl. 1 pp. 515-515. Paper: P1975, 1p. (2018)

HORVATH O, DERES L, EROS K, **ORDOG K**, HABON T, SUMEGI B, TOTH K, HALMOSI R. Oxidative stress-induced changes in mitochondrial dynamics of cardiomyocytes in cell culture. CARDIOLOGIA HUNGARICA Supplementum C, C38 (2018)

ORDOG K, DERES L, EROS K, HORVATH O, HABON T, SUMEGI B, TOTH K, HALMOSI R. Effect of BGP-15 treatment on hypertension induced cardiac remodeling in an in vivo SHR model. CARDIOLOGIA HUNGARICA Supplementum C, C34 (2018)